Figure 5 Comparison of Antigen Ki-67 (Ki-67) and Topoisomerase (Topo) IIα Expression Between the 2 Groups of Luminal Breast Cancer Tissue Samples. (A) Comparison of Ki-67 Between the 2 Groups. (B) Comparison of Topo IIα Between the 2 Groups. Differences Between Groups Were Analyzed Using the Mann–Whitney *U* Test. $P < .05$ Was Considered to Indicate Statistical Significance

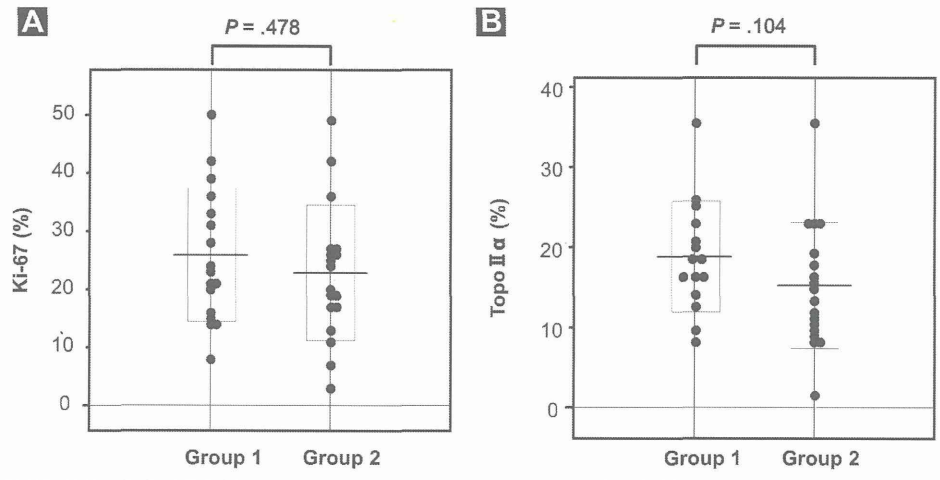

Correlation Between $CD44^+/CD24^-$/Hoechst Cell Proportions and Sphere-Forming Ability

Although several surface antigens or side populations determined using FACS analysis have been reported as markers to distinguish CSCs, this method is not suitable for analyzing many clinical samples because only small surgical specimens are frequently obtained. We used CD44/CD24/Hoechst combination staining, and the populations that showed $CD44^+/CD24^-$/$Hoechst^-$ cells were considered to be a CSC-enriched populations in breast cancer. The staining patterns of CD44, CD24, and Hoechst 33342 varied among the samples. For example, mammospheres prepared from patient 125 showed a predominance of $CD44^+$ cells; and those from patient 108 showed a predominance of $CD24^+$ cells. The staining pattern of mammospheres from patient 114 exhibited intrasphere heterogeneity (Figure 2A). The correlation between $CD44^+/CD24^-$/$Hoechst^-$ cell proportions in mammospheres and sphere-forming ability was significantly positive ($r = 0.34$; $P < .01$) (Figure 2B). This result indicates that the combination of these 3 markers could be appropriate for partial assessment of breast cancer stemness.

Expression of Cancer Stemness-Related Genes in Mammospheres

To analyze the stemness properties of mammospheres prepared from primary breast cancers, the expression levels of stemness-related genes were analyzed. Each relative mRNA expression level was calculated by dividing the expression level by the average level of all samples. The relative *OCT4* and *NANOG* mRNA expression levels showed strong positive correlation ($r = 0.936$; $P < .01$) (Figure 3A), whereas the *NANOG* and *KLF4* mRNA expression levels were negatively correlated ($r = -0.296$; $P = .05$; Figure 3B). To investigate the relative expression levels especially in luminal-type breast cancers, the levels were recalculated using the average of luminal-type breast cancers because the relative *NANOG* and *KLF4* mRNA expression levels were significantly greater in nonluminal type than in luminal type breast cancers (Figure 3C and D).

Classification of Luminal Type Breast Cancers and Comparison of Stemness Properties Between 2 Groups

We classified luminal type breast cancer into 2 groups according to the ratio of relative *NANOG* and *KLF4* mRNA expression levels (Figure 4A; ie, group 1 expressed predominantly *NANOG* mRNA in mammospheres prepared from luminal-type breast cancers). In contrast, group 2 predominantly expressed *KLF4*.

The stemness properties were assessed according to sphere-forming ability and the $CD44^+/CD24^-$/$Hoechst^-$ cell proportion. Although the differences in sphere-forming ability were not clear (Figure 4B), the proportion of $CD44^+/CD24^-$/$Hoechst^-$ cells was significantly greater in group 1 than in group 2 (Figure 4C). The average $CD44^+/CD24^-$/$Hoechst^-$ cell proportion was 2.7 times greater in group 1 than in group 2. These results indicated that the mammospheres in group 1 had higher stemness properties than those in group 2.

Comparison of Ki-67 and Topo IIα Expression Between 2 Groups

The value of Ki-67 is widely used to distinguish between luminal A and luminal B. In addition, topo IIα is considered an index of cell-dividing ability. Ki-67 and topo IIα expression tended to be greater in group 1 than in group 2 (Figure 5). However, there was no clear boundary to distinguish the 2 groups according to expression levels. This result indicated that the groups divided according to mammosphere stemness properties

Table 1 Correlation of Clinicopathological Factors Between the 2 Luminal Breast Cancer Groups

Variable	n	Group 1		Group 2		P
		n	%	n	%	
Age, Years						.063
<57 (Median)	17	11	64.7	6	35.3	
	18	6	33.3	12	66.7	
Histological Grade						.146
3	10	7	70.0	3	30.0	
1 and 2	25	10	40.0	15	60.0	
Stage						.485
III	2	0	0.0	2	100.0	
I and II	31	16	51.6	15	48.4	
Tumor Size, cm						.521
0-2	22	11	50.0	11	50.0	
>2 to 5	12	5	41.7	7	58.3	
>5	1	1	100.0	0	0.0	
LVI						.395
Positive	17	7	41.2	10	58.8	
Negative	18	10	55.6	8	44.4	
Lymph Node Status						.229
Positive	16	6	37.5	10	62.5	
Negative	19	11	57.9	8	42.1	
PR						.603
Positive	32	15	46.9	17	53.1	
Negative	3	2	66.7	1	33.3	
HER2						1.000
Positive	3	1	33.3	2	66.7	
Negative	32	16	50.0	16	50.0	
p53						<.05
Positive	9	7	77.8	2	22.2	
Negative	24	8	33.3	16	66.7	

Abbreviations: LVI = lymphovascular invasion; PR = progesterone receptor.

were different from those divided according to the Ki-67 or topo IIα index.

Comparison of Clinicopathological Factors Between the 2 Groups

Clinicopathological factors between the 2 luminal-type breast cancer groups were compared. Group 1 significantly correlated with p53 high expression; in addition, the patients from which the tissue samples were taken tended to be younger and the samples exhibited higher histological grade than those in group 2. There were no significant differences in the other parameters (Table 1).

Estrogen Response Element Activities and ER Expression in Mammospheres Prepared From Luminal Type Breast Cancers

We previously reported that we used the ERE-GFP assay to analyze ER activity in clinical specimens, such as those from endometrial cancers and primary breast cancers.[31,32] In the present study, this method was used to analyze the ER activities of mammospheres prepared from luminal type breast cancers. In addition, surface CD44 antigen staining was performed. Moreover, we analyzed the ER expression of the mammospheres. In the mammospheres of patient 91, ERE activities induced by E2 and ER expression were observed. However, in the mammospheres of patient 131, neither ERE activities nor ER expression was observed although the luminal type breast cancer was ER^+ in the immunohistological analysis. In specimens of triple-negative breast cancer, patient 101, no GFP or ER expression was detected, as expected (Figure 6).

Among 9 patient samples analyzed for ER activities, the mammospheres prepared from 6 samples maintained ER activities and exhibited ER expression. In contrast, 3 samples lacked ER activities although they were taken from luminal type breast cancers (Table 2). Moreover, approximately one-third of these luminal type cases were categorized into group 1, which had high stemness.

Discussion

Evaluation of stemness properties in breast cancer is an important tool for prediction of prognosis and selection

Figure 6 Estrogen Response Element (ERE) Activities and Estrogen Receptor (ER) Expression of Mammospheres. (A) To Evaluate ERE Activities, Mammospheres Cultured > 14 Days Were Used to Eliminate Endogenous Estrogen. Cells With ERE Activities Are Indicated by Green Fluorescent Protein-Positive Cells (Green), and CD44-Positive Cells Are Indicated by Red. Cellular ER and CD44 Expressions Are Shown by Staining With Anti-ER Antibody (Green) and Anti-CD44 Antibody (Red) of Mammospheres Cultured for 7 Days

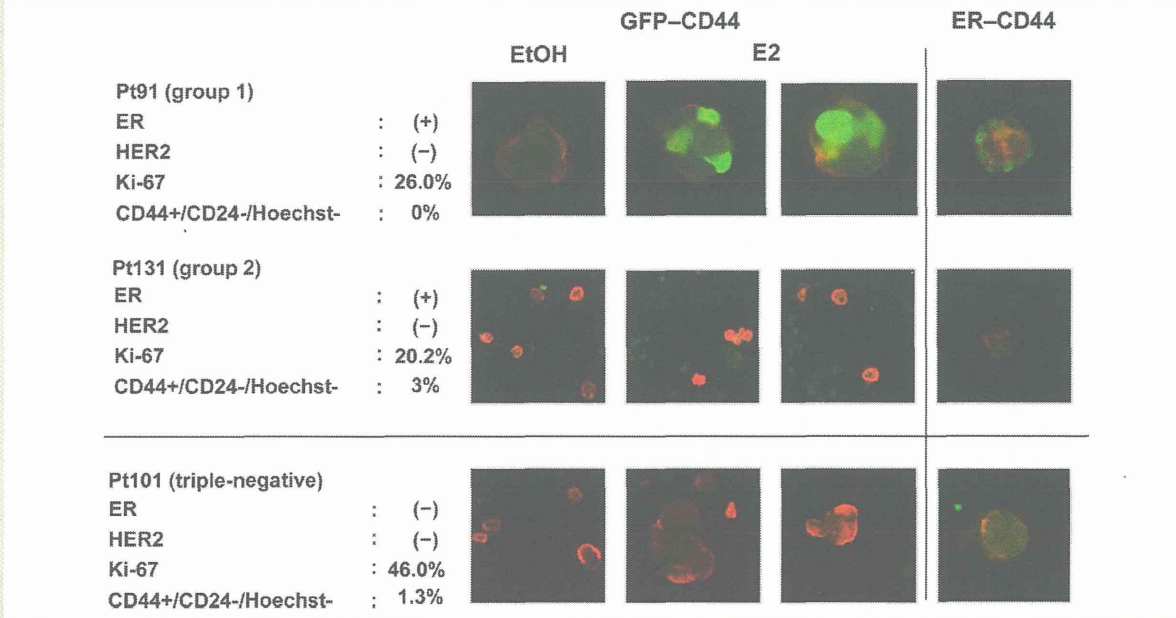

of treatment because CSCs are thought to be associated with cancer progression, recurrence, metastasis, and drug susceptibility. To date, this issue has been studied mostly using immunohistochemical analysis with antibodies against CSC surface markers, such as CD44 and CD24, of paraffin-embedded clinical samples. However, no significant conclusions have been obtained in these immunohistochemical studies. In our study, the stemness properties of tumor tissues were evaluated using mammospheres prepared from clinical samples because CSCs are enriched in mammospheres cultured using low-attachment surface plates. Especially, we explored the possibility of new subclassifications in luminal type breast cancer according to stemness properties.

Sphere-forming ability and the proportion of $CD44^+/CD24^-/Hoechst^-$ cells were positively correlated. The proportion of $CD44^+/CD24^-/Hoechst^-$ cells ranged from 0% to 5%. Moreover, the correlation between *OCT4* and *NANOG* expression was strongly positive. Conversely, there was a negative correlation between *KLF4* and *NANOG*. In these parameters, we focused on the inverse correlation between the *NANOG* and *KLF4* mRNA

Table 2 Estrogen Response Element Activities and ER Expression of the Mammospheres

	Mammosphere					IHC					
	ERE-GFP	ER	Number of Spheres	$CD44^+/CD24^-/Hoechst^-$, %	Group	ER (Allred score)	PR (Allred score)	HER2	p53	Ki-67, %	Topo IIα, %
Pt121	+	+	233	3.6	1	8	7	−	−	16.4	9.8
Pt125	+	+	152	4.9	1	8	7	−	+	31.4	23.0
Pt133	+	+	151	4.1	1	7	8	−	+	36.0	13.0
Pt091	+	+	228	0.0	2	8	7	−	−	26.0	19.4
Pt100	+	+	21	1.9	2	8	7	−	−	24.0	13.6
Pt161	+	+	84	0.0	2	7	7	−	−	20.2	23.4
Pt131	−	−	14	3.0	1	7	8	−	+	20.2	16.2
Pt094	−	ND	62	1.6	2	8	6	−	−	2.8	1.3
Pt099	−	−	75	1.1	2	8	7	−	+	41.8	23.0

Abbreviations: ER = estrogen receptor; ERE = estrogen response element; GFP = green fluorescent protein; ND = not done.

expression levels. Ben-Porath et al previously reported that the activation targets of NANOG, OCT4, sex determining region Y-box 2, and proto-oncogene c-Myc were more frequently overexpressed in poorly differentiated tumors than in well differentiated tumors.[24] In addition, the *NANOG* mRNA expression level was greater in mammospheres prepared from nonluminal breast cancer than in those from luminal type breast cancers, as expected. To compare the expression levels of stemness-related genes only in luminal type breast cancers, nonluminal breast cancer was excluded and luminal type breast cancers were separated into 2 groups (Figure 4A). Group 1 exhibited greater expression of *NANOG* mRNA in luminal type breast cancers, had a significantly greater proportion of $CD44^+/CD24^-/Hoechst^-$ cells, and exhibited a greater degree of stemness properties than group 2. In contrast, the sphere-forming ability was not significantly different between the 2 groups. This suggested that the proportion of $CD44^+/CD24^-/Hoechst^-$ cells was a better marker than sphere-forming ability for evaluation of the stemness properties of tumor tissues.

Group 1 was associated with younger patient age, significantly greater expression of p53, and tended to exhibit greater histological grade. It is well known that p53 is essential for normal cellular homeostasis.[33-35] Abnormal nuclear accumulation of p53 assessed immunohistochemically is used as a marker for the presence of mutated p53 because the protein half-life time becomes longer. In our study, p53 expression was positive in 80% of luminal type cancer group 1. This positive rate was greater than that given in a previous report in which *tumor suppressor protein p53* gene mutation was observed in 84% of the basal-like, 12% of the luminal A, and 32% of the luminal B subtypes.[36]

Accumulation of p53 was associated with a high tumor proliferation rate and poor clinical outcome in node-negative breast cancer patients.[37] Moreover, according to Yamamoto M et al, p53 accumulation predicted resistance to endocrine therapy and decreased post-relapse survival in metastatic breast cancer.[38] During differentiation, the interaction between p53 and NANOG was previously revealed by Lin et al,[39] and Akdemir et al.[40] These results suggest that this classification, according to the ratio of relative *NANOG* and *KLF4* mRNA expression levels, reflects the high stemness properties and relatively high *NANOG* expression and that positive p53 expression in immunohistochemical analysis could be a marker associated with stemness properties of tumor tissues in luminal breast cancer.

For luminal type breast cancer, ERE activity or ER expression is an important factor for evaluation of the sensitivity to endocrine therapies that target ER or E2 synthesis. The lack or low expression of ERα in normal breast stem/progenitor cells has previously been reported,[41] but expression of ERα in CSCs of luminal type breast cancer is not clear. In our study, 6 of 9 tissue samples showed ERE activity in mammospheres, and 3 lacked ER activity against E2 even though the samples were taken from luminal type breast cancer. Staining patterns were heterogeneous. Although there was a possibility that these ERE^- or ER^+ cells were derived from CSCs during sphere culture, the results suggested that there were different types of CSCs in luminal type breast cancer. The first CSC type is ERE^+ and ER^+ or can produce ERE^+ and ER^+ cells, and the second CSC type is ERE^- and ER^-. Simões et al reported that *NANOG*, *OCT4*, and *sex determining region Y-box 2* overexpression in human breast cancer cell line MCF7 reduced ER expression.[42] In our results, a clear relationship between ERE activities or ER expression and *NANOG* expression in mammospheres was not shown, but the results suggested the heterogeneity of CSCs in luminal type breast cancer. Because the tumors derived from CSCs exhibit different properties, they might show different responses to endocrine therapy. Consequently, understanding the characteristics of CSCs in luminal type breast cancer is thought to be important.

Clinically, immunohistochemical analysis has been used as an alternative method to define breast cancer subtypes because of the complexity of microarray analysis. Ki-67 and topo IIα have been reported to be proliferation markers[43,44] and are often used to classify the subtype of luminal cancer tumors that are ER^+ and $HER2^-$, and tumors that exhibit Ki-67 of $< 14\%$ are usually classified as luminal B in breast cancer. In our study, Ki-67 tended to be greater in group 1 than in group 2, but there was no clear distinction. This result suggests that the Ki-67 level might not be proportional to a greater degree of stemness properties.

Although long-term follow-up is required to determine whether classification according to mammosphere stemness properties is useful for the prediction of prognosis and the evaluation of sensitivity to endocrine therapy, this could be a novel method for the subclassification of luminal type breast cancer. It is easy to evaluate the stemness-related gene expression of many samples using RT-PCR. However, mammospheres culture is often clinically complicated. A new convenient marker that reflects mammosphere stemness properties and ERE activities is needed for analyzing many samples clinically.

Conclusion

Differences in ERE activity might be associated with the effectiveness of endocrine therapy. Assessment of mammosphere stemness properties could be a useful and novel approach to the subclassification of luminal type breast cancers.

Clinical Practice Points

- Although endocrine therapies that target ER or E2 synthesis have led to marked improvement in disease-free and overall survival in luminal type breast cancer, Approximately 30% of luminal type breast cancers show poor response to endocrine therapy.
- Luminal type breast cancers are heterogeneous.
- It is thought that the cancer stemness cells have a pivotal role in recurrence and metastasis because of their characteristic of resistance to chemotherapy and radiotherapy.
- Assessment of mammospheres stemness properties could be a useful for prediction of prognosis and the evaluation of sensitivity to endocrine therapy.

Acknowledgments

This study was supported in part by a Grant-in-Aid for Scientific Research from the Ministry of Education, Culture, Sports, Science and Technology, Japan (22790520); a Grant-in-Aid for Cancer Research from the Ministry of Health, Labor and Welfare, Japan (H24-3-006); the Program for Promotion of Fundamental Studies in Health Science of the National Institute of Biomedical

Innovation (09-02); and a grant from the Smoking Research Foundation.

Disclosure

The authors have stated that they have no conflicts of interest.

References

1. Perou CM, Sørlie T, Eisen MB, et al. Molecular portraits of human breast tumours. *Nature* 2000; 406:747-52.
2. Sørlie T, Perou CM, Tibshirani R, et al. Gene expression patterns of breast carcinomas distinguish tumor subclasses with clinical implications. *Proc Natl Acad Sci U S A* 2001; 98:10869-74.
3. Goldhirsch A, Wood WC, Coates AS, et al. Strategies for subtypes—dealing with the diversity of breast cancer: highlights of the St. Gallen International Expert Consensus on the Primary Therapy of Early Breast Cancer 2011. *Ann Oncol* 2011; 22:1736-47.
4. Rody A, Karn T, Ruckhäberle E, et al. Gene expression of topoisomerase II alpha (TOP2A) by microarray analysis is highly prognostic in estrogen receptor (ER) positive breast cancer. *Breast Cancer Res Treat* 2009; 113:457-66.
5. Fritz P, Cabrera CM, Dippon J, et al. c-erbB2 and topoisomerase II alpha protein expression independently predict poor survival in primary human breast cancer: a retrospective study. *Breast Cancer Res* 2005; 7:R374-84.
6. Børresen-Dale AL. TP53 and breast cancer. *Hum Mutat* 2003; 21:292-300.
7. Olivier M, Langerød A, Carrieri P, et al. The clinical value of somatic TP53 gene mutations in 1,794 patients with breast cancer. *Clin Cancer Res* 2006; 12: 1157-67.
8. Veronesi U, Cascinelli N, Greco M, et al. A reappraisal of oophorectomy in carcinoma of the breast. *Ann Surg* 1987; 205:18-21.
9. Li X, Lewis MT, Huang J, et al. Intrinsic resistance of tumorigenic breast cancer cells to chemotherapy. *J Natl Cancer Inst* 2008; 100:672-9.
10. Phillips TM, McBride WH, Pajonk F. The response of CD24(−/low)/CD44+ breast cancer-initiating cells to radiation. *J Natl Cancer Inst* 2006; 98:1777-85.
11. Goodell MA, Brose K, Paradis G, Conner AS, Mulligan RC. Isolation and functional properties of murine hematopoietic stem cells that are replicating in vivo. *J Exp Med* 1996; 183:1797-806.
12. Ginestier C, Hur MH, Charafe-Jauffret E, et al. ALDH1 is a marker of normal and malignant human mammary stem cells and a predictor of poor clinical outcome. *Cell Stem Cell* 2007; 1:555-67.
13. Al-Hajj M, Wicha MS, Benito-Hernandez A, Morrison SJ, Clarke MF. Prospective identification of tumorigenic breast cancer cells. *Proc Natl Acad Sci U S A* 2003; 100:3983-8.
14. Ponti D, Costa A, Zaffaroni N, et al. Isolation and in vitro propagation of tumorigenic breast cancer cells with stem/progenitor cell properties. *Cancer Res* 2005; 65:5506-11.
15. Singh SK, Clarke ID, Terasaki M, et al. Identification of a cancer stem cell in human brain tumors. *Cancer Res* 2003; 63:5821-8.
16. Collins AT, Berry PA, Hyde C, Stower MJ, Maitland NJ. Prospective identification of tumorigenic prostate cancer stem cells. *Cancer Res* 2005; 65: 10946-51.
17. Patrawala L, Calhoun T, Schneider-Broussard R, et al. Highly purified CD44+ prostate cancer cells from xenograft human tumors are enriched in tumorigenic and metastatic progenitor cells. *Oncogene* 2006; 25:1696-708.
18. Ricci-Vitiani L, Lombardi DG, Pilozzi E, et al. Identification and expansion of human colon-cancer-initiating cells. *Nature* 2007; 445:111-5.
19. Li C, Heidt DG, Dalerba P, et al. Identification of pancreatic cancer stem cells. *Cancer Res* 2007; 67:1030-7.
20. Lengerke C, Fehm T, Kurth R, et al. Expression of the embryonic stem cell marker SOX2 in early-stage breast carcinoma. *BMC Cancer* 2011; 11:42.
21. Ezeh UI, Turek PJ, Reijo RA, Clark AT. Human embryonic stem cell genes OCT4, NANOG, STELLAR, and GDF3 are expressed in both seminoma and breast carcinoma. *Cancer* 2005; 104:2255-65.
22. Yu F, Li J, Chen H, et al. Kruppel-like factor 4 (KLF4) is required for maintenance of breast cancer stem cells and for cell migration and invasion. *Oncogene* 2011; 30: 2161-72.
23. Rodda DJ, Chew JL, Lim LH, et al. Transcriptional regulation of nanog by OCT4 and SOX2. *J Biol Chem* 2005; 280:24731-7.
24. Takahashi K, Yamanaka S. Induction of pluripotent stem cells from mouse embryonic and adult fibroblast cultures by defined factors. *Cell* 2006; 126:663-76.
25. Ben-Porath I, Thomson MW, Carey VJ, et al. An embryonic stem cell-like gene expression signature in poorly differentiated aggressive human tumors. *Nat Genet* 2008; 40:499-507.
26. Miller KA, Eklund EA, Peddinghaus ML, et al. Kruppel-like factor 4 regulates laminin alpha 3A expression in mammary epithelial cells. *J Biol Chem* 2001; 276: 42863-8.
27. Pandya AY, Talley LI, Frost AR, et al. Nuclear localization of KLF4 is associated with an aggressive phenotype in early-stage breast cancer. *Clin Cancer Res* 2004; 10:2709-19.
28. Nagata T, Shimada Y, Sekine S, et al. Prognostic significance of NANOG and KLF4 for breast cancer. *Breast Cancer* 2014; 21:96-101.
29. Akaogi K, Nakajima Y, Ito I, et al. KLF4 suppresses estrogen-dependent breast cancer growth by inhibiting the transcriptional activity of ER alpha. *Oncogene* 2009; 28:2894-902.
30. Bane A, Viloria-Petit A, Pinnaduwage D, Mulligan AM, O'Malley FP, Andrulis IL. Clinical-pathologic significance of cancer stem cell marker expression in familial breast cancers. *Breast Cancer Res Treat* 2013; 140:195-205.
31. Matsumoto M, Yamaguchi Y, Seino Y, et al. Estrogen signaling ability in human endometrial cancer through the cancer-stromal interaction. *Endocr Relat Cancer* 2008; 15:451-63.
32. Gohno T, Seino Y, Hanamura T, et al. Individual transcriptional activity of estrogen receptors in primary breast cancer and its clinical significance. *Cancer Med* 2012; 1:328-37.
33. Donehower LA, Harvey M, Slagle BL, et al. Mice deficient for p53 are developmentally normal but susceptible to spontaneous tumours. *Nature* 1992; 356:215-21.
34. Haupt S, Berger M, Goldberg Z, Haupt Y. Apoptosis - the p53 network. *J Cell Sci* 2003; 116:4077-85.
35. Attardi LD, Jacks T. The role of p53 in tumour suppression: lessons from mouse models. *Cell Mol Life Sci* 1999; 55:48-63.
36. Cancer Genome Atlas Network. Comprehensive molecular portraits of human breast tumours. *Nature* 2012; 490:61-70.
37. Allred DC, Clark GM, Elledge R, et al. Association of p53 protein expression with tumor cell proliferation rate and clinical outcome in node-negative breast cancer. *J Natl Cancer Inst* 1993; 85:200-6.
38. Yamamoto M, Hosoda M, Nakano K, et al. p53 accumulation is a strong predictor of recurrence in estrogen receptor-positive breast cancer patients treated with aromatase inhibitors. *Cancer Sci* 2014; 105:81-8.
39. Lin T, Chao C, Saito S, et al. p53 induces differentiation of mouse embryonic stem cells by suppressing Nanog expression. *Nat Cell Biol* 2005; 7:165-71.
40. Akdemir KC, Jain AK, Allton K, et al. Genome-wide profiling reveals stimulus-specific functions of p53 during differentiation and DNA damage of human embryonic stem cells. *Nucleic Acids Res* 2014; 42:205-23.
41. Clayton H, Titley I, Vivanco MD. Growth and differentiation of progenitor/stem cells derived from the human mammary gland. *Exp Cell Res* 2004; 297:444-60.
42. Simões BM, Piva M, Iriondo O, et al. Effects of estrogen on the proportion of stem cells in the breast. *Breast Cancer Res Treat* 2011; 129:23-35.
43. Gerdes J, Lemke H, Baisch H, Wacker HH, Schwab U, Stein H. Cell cycle analysis of a cell proliferation-associated human nuclear antigen defined by the monoclonal antibody Ki-67. *J Immunol* 1984; 133:1710-5.
44. Lynch BJ, Guinee DG Jr, Holden JA. Human DNA topoisomerase II-alpha: a new marker of cell proliferation in invasive breast cancer. *Hum Pathol* 1997; 28: 1180-8.

SCIENTIFIC REPORTS

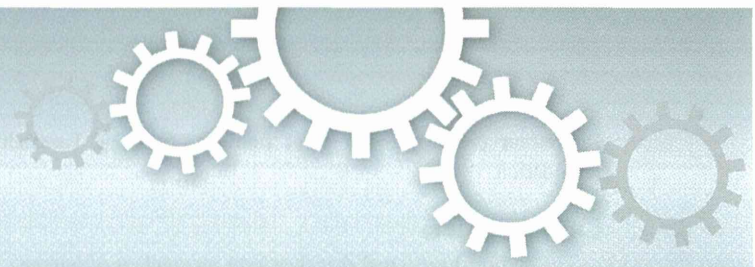

OPEN

SUBJECT AREAS:
BREAST CANCER
CELL INVASION
CANCER MICROENVIRONMENT

Received
17 March 2014

Accepted
28 October 2014

Published
17 November 2014

Correspondence and requests for materials should be addressed to Y.M. (miki.mgen@mri.tmd.ac.jp)

Periostin suppression induces decorin secretion leading to reduced breast cancer cell motility and invasion

Toshiyuki Ishiba[1,2], Makoto Nagahara[2], Tsuyoshi Nakagawa[2], Takanobu Sato[2], Toshiaki Ishikawa[2], Hiroyuki Uetake[2], Kenichi Sugihara[2], Yoshio Miki[1,3] & Akira Nakanishi[1]

[1]Department of Molecular Genetics, Medical Research Institute, Tokyo Medical and Dental University (TMDU), [2]Department of Surgical Oncology, Tokyo Medical and Dental University (TMDU), [3]Department of Molecular Diagnosis, Cancer Institute, The Japanese Foundation of Cancer Research (JFCR).

The ability of cancer cells to metastasize is dependent on the interactions between their cell-surface molecules and the microenvironment. However, the tumor microenvironment, especially the cancer-associated stroma, is poorly understood. To identify proteins present in the stroma, we focused on phyllodes tumors, rare breast tumors that contain breast stromal cells. We compared the expression of proteins between phyllodes tumor and normal tissues using an iTRAQ-based quantitative proteomic approach. Decorin was expressed at reduced levels in phyllodes tumor tissues, whereas periostin was upregulated; this result was validated by immunohistochemical analysis of phyllodes tumors from 35 patients. Additionally, by immunoprecipitation and mass spectrometry, we confirmed that decorin forms a complex with periostin in both phyllodes tumors and BT-20 breast cancer cells. Following siRNA-mediated knockdown of periostin in T-47D cells, secreted decorin in the culture medium could be detected by multiple reaction monitoring (MRM). Furthermore, periostin knockdown in BT-20 cells and overexpression of decorin in MDA-MB-231 cells inhibited cell motility and invasion. Our results reveal the molecular details of the periostin–decorin complex in both phyllodes tumor tissues and breast cancer cells; this interaction may represent a novel target for anti-cancer therapy.

The tumor microenvironment plays a critical role in cancer progression. The stromal and epithelial cells that constitute the tumor microenvironment strongly influence tumor proliferation, invasion, and metastasis, and the phenotypes of tumors are largely determined by interactions between cancer cells and their microenvironment[1–3]. Analyses of cancerous stroma are crucial to improving our understanding of cancer.

Recent studies have shown that periostin and decorin are components of the extracellular matrix that affect the biology of various types of cancer[4,5]. Periostin, also known as OSF-2, is a 93-kDa matrix N-glycoprotein. Upregulation of periostin has been observed in many human tumors, including cancers of the lung[6,7], colon[8], skin[9], pancreas[10], thyroid[11], ovary[12], breast[13], and prostate[14]; periostin overexpression is associated with increased tumor invasion and accelerated progression[15,16]. Furthermore, high stromal periostin expression is a prognostic factor associated with reduced progression-free survival[12]. Gillan *et al.* reported that periostin interacts with integrin receptors[17]. Purified recombinant periostin supported the attachment of human ovarian surface epithelia (HOSE) and human ovarian carcinoma cells (Sk-ov-3). Sk-ov-3 cells express the β1, αVβ3, and αVβ5 integrins. Attachment of Sk-ov-3 cells to a periostin-coated plate was inhibited by anti-αVβ3 or anti-αVβ5 antibody, whereas function-blocking antibodies against β1 integrins inhibited the attachment of Sk-ov-3 cells to fibronectin. On the other hand, periostin overexpressed in cancer-associated fibroblasts (CAFs) is a key component of primary tumor niche and supports cancer cell proliferation[18]; likewise, in colon cancer, periostin secreted by CAFs supports the growth of epithelial components[19].

Small leucine-rich proteoglycans (SLRPs) are components of the extracellular matrix, which is altered in the environment surrounding a tumor. SLRPs such as decorin, lumican, and biglycan are expressed in the vicinity of colon, pancreas, breast, and prostate cancers[20–22]. Decorin is a proteoglycan, on average 90–140 kDa in molecular weight, consisting of a 40-kDa protein core containing leucine repeats conjugated to a glycosaminoglycan chain consisting of either chondroitin sulfate or dermatan sulfate. Relative to adjacent normal stroma, decorin expression is downregulated in fibroblast-like cells within the stroma surrounding human breast tumors[20]. Furthermore,

decorin-expressing tumor xenografts grow at significantly lower rates and exhibit significantly suppressed neovascularization[23]. Decorin binds collagen I, regulates fibrillogenesis[24,25], and protects collagen fibrils from proteolytic cleavage by various collagenases[26].

Decorin has recently emerged as a potential natural anticancer agent produced by normal cells[27]. Specifically, decorin neutralizes the bioactivity of transforming growth factor-beta1 (TGF-β1), an autocrine factor that stimulates the growth of cancer cells[28,29]. Collectively, the set of proteins that interact with decorin (the 'interactome') generates a powerful antitumorigenic signal by potently repressing tumor cell proliferation, survival, migration, and angiogenesis[30]. Fibroblasts secrète several components of the extracellular matrix, including decorin[31,32], and also play important roles in influencing progression toward malignancy[33]. Therefore, fibroblasts are key determinants of the malignant progression of cancer, and thus represent an important target for cancer therapies[34].

In this study, we focused on phyllodes tumors, which are composed of epithelial and cellular stromal components of the breast. We compared tissue-specific protein expression in phyllodes tumor and normal tissues by iTRAQ (isobaric tag for relative and absolute quantitation) and tandem mass spectroscopy. These analyses revealed that decorin was expressed at lower levels, whereas periostin expression was upregulated, in phyllodes tumor tissues and cancer cells. Furthermore, we characterized the periostin–decorin complex. In particular, we found that knockdown of periostin results in translocation of decorin from the cytoplasm to the extracellular space, leading to the inhibition of cancer cell migration and invasion.

Results

Periostin upregulation and decorin downregulation in phyllodes tumor tissue. Cancer stroma consists mainly of cancer-associated fibroblasts (CAFs), which affect aspects of the tumor microenvironment such as angiogenesis, invasion, and metastasis. CAFs promote tumor progression in breast cancer, but the details of their role remain unclear, primarily because the collection of CAFs from cancer tissue is technically difficult. Therefore, in this study we focused on phyllodes tumors, which consist of breast stromal and epithelial cells. We used the iTRAQ-based quantitative proteomic approach to identify proteins that were differentially expressed between phyllodes tumor and normal tissues. As shown in Supplementary Figure S1, a total of 2041 proteins in case 1, 2338 proteins in case 2, and 4281 proteins in case 3 were identified by ProteinPilot. Of the identified proteins, 99.9% in case 1, 99.8% in case 2, and 99.6% in case 3 were labeled with iTRAQ tags. Next, we selected proteins that were at least 3-fold more abundant in one of these tissue types (tag 114/tag 117 $>$ 3 for proteins enriched in normal tissue, or tag 117/tag 114 $>$ 3 for proteins enriched in tumor tissue). We set a cutoff of 3-fold according to the method described by Juling Ji et al[35]. A total of 101 proteins were detected multiple times in three serial measurements from the same KCl concentration fractions (Supplementary Table S1). Finally, from among the proteins detected in all three cases, we selected five proteins enriched in normal tissues and two proteins in phyllodes tumor tissues. Decorin, mimecan, hemoglobin subunit alpha, hemoglobin subunit beta, and keratin type I cytoskeletal 19 were upregulated in normal tissue, whereas periostin and versican core protein were upregulated in phyllodes tumor tissue (Supplementary Figure S1). Periostin and decorin are components of the extracellular matrix. Periostin upregulation has been reported in many types of cancer, and it is consequently defined as a tumor-enhancing factor[10,17,36,37]. On the other hand, decorin upregulation inhibits tumor growth by antagonizing tumor angiogenesis[30]. Both proteins have recently been discussed as potential targets for stroma-targeted anticancer therapy[17,30]. Accordingly, we focused our subsequent analyses on decorin and periostin. In all three cases, decorin was expressed at higher levels in normal tissues than in phyllodes tumors, whereas periostin was upregulated in phyllodes tumor, as confirmed by immunoblot analysis (Figure 1a). Immunohistochemistry revealed that decorin and periostin were localized in the extracellular matrix (Figure 1b).

Decorin is upregulated in normal tissue, and periostin is upregulated in phyllodes tumor tissue, from cancer patients. To validate the accuracy of the results described above, we performed immunohistochemical analysis to examine the levels of decorin and periostin in tumor and normal tissues from 35 phyllodes tumor patients. Decorin expression in normal tissues was higher than in tumor tissues ($P < 0.001$, Wilcoxon signed-rank test; $n = 35$) (Figure 2a), whereas periostin expression was lower in normal tissues ($P = 0.005$, Wilcoxon signed-rank test; $n = 35$) (Figure 2b). Our data suggests that downregulation of decorin and upregulation of periostin are correlated with malignant progression of tumors.

Next, we verified the expression of both proteins in phyllodes tumors ($n = 35$) and breast fibroadenomas ($n = 37$) by immunohistochemical analysis. Fibroadenomas, the most common benign breast tumors, arise from intralobular fibrous tissue. Decorin was present at higher levels in fibroadenomas than in phyllodes tumors ($P = 0.009$, Mann-Whitney U test; $n = 37, 35$) (Figure 2c), whereas periostin was present at lower levels in fibroadenomas ($P = 0.007$, Mann-Whitney U test; $n = 37, 35$) (Figure 2d). These results suggest that it might be possible to distinguish phyllodes tumors and fibroadenomas by comparing the relative expression levels of decorin and periostin.

Complex between periostin and decorin in phyllodes tumor tissue. To identify decorin- or periostin-binding proteins in normal and phyllodes tumor tissues, we immunoprecipitated both proteins, and subjected the immunoprecipitates to SDS-PAGE and silver staining. Gel bands representing differences between normal and phyllodes tumor tissue were cut out and subjected to in-gel trypsin digestion and mass spectrometry (Figure 2e and 2f). Thirteen proteins, including periostin, were identified in the anti-decorin immunoprecipitates (Figure 2e and Supplementary Table S2), and twelve proteins, including decorin, were detected in the anti-periostin immunoprecipitates (Figure 2f and Supplementary Table S2). Protein identifications were accepted on the basis of peptide identifications with greater than 95.0% confidence.

Silencing of periostin by RNA interference induces secretion of decorin from the cell. We next sought to investigate the functional significance of the interaction between decorin and periostin, both of which are secreted proteins. First, we confirmed that both proteins were expressed in the breast cancer cell lines BT-20 and T-47D; in other cell lines we examined (MCF7, MDA-MB231, and HeLa S3), periostin was present but decorin was not (Figure 3a and Supplementary Figure S2). By co-immunoprecipitation of these proteins from BT-20 lysates, we confirmed that endogenous decorin and periostin interacted in these cells, either directly or indirectly (Figure 3b and Supplementary Figure S3). Immunofluorescence confocal microscopy revealed that decorin and periostin colocalized in BT-20 cells (Figure 3c). Decorin and periostin are components of the extracellular matrix[4,5]. We hypothesized that decorin is secreted into the culture medium following treatment with siRNA-periostin. To test this hypothesis, we analyzed secreted decorin in the culture medium by immunoprecipitation, followed by immunoblotting using an anti-decorin antibody, but this antibody was highly cross-reactive and yielded many nonspecific bands(Figure 3d). To overcome this technical obstacle, we used multiple reaction monitoring (MRM) mass spectrometry. In this assay, 5 fmol of standard peptides [VSPGAFTPLVK ($^{13}C_6$, $^{15}N_2$) or DLPPDTTLLDLQNNK ($^{13}C_6$, $^{15}N_2$)] was separated by nano-LC, and the MRM transitions were monitored. The peptides were delivered in 5% (v/v) acetonitrile at a concentration of 5 pmol/μl. Figure 4a

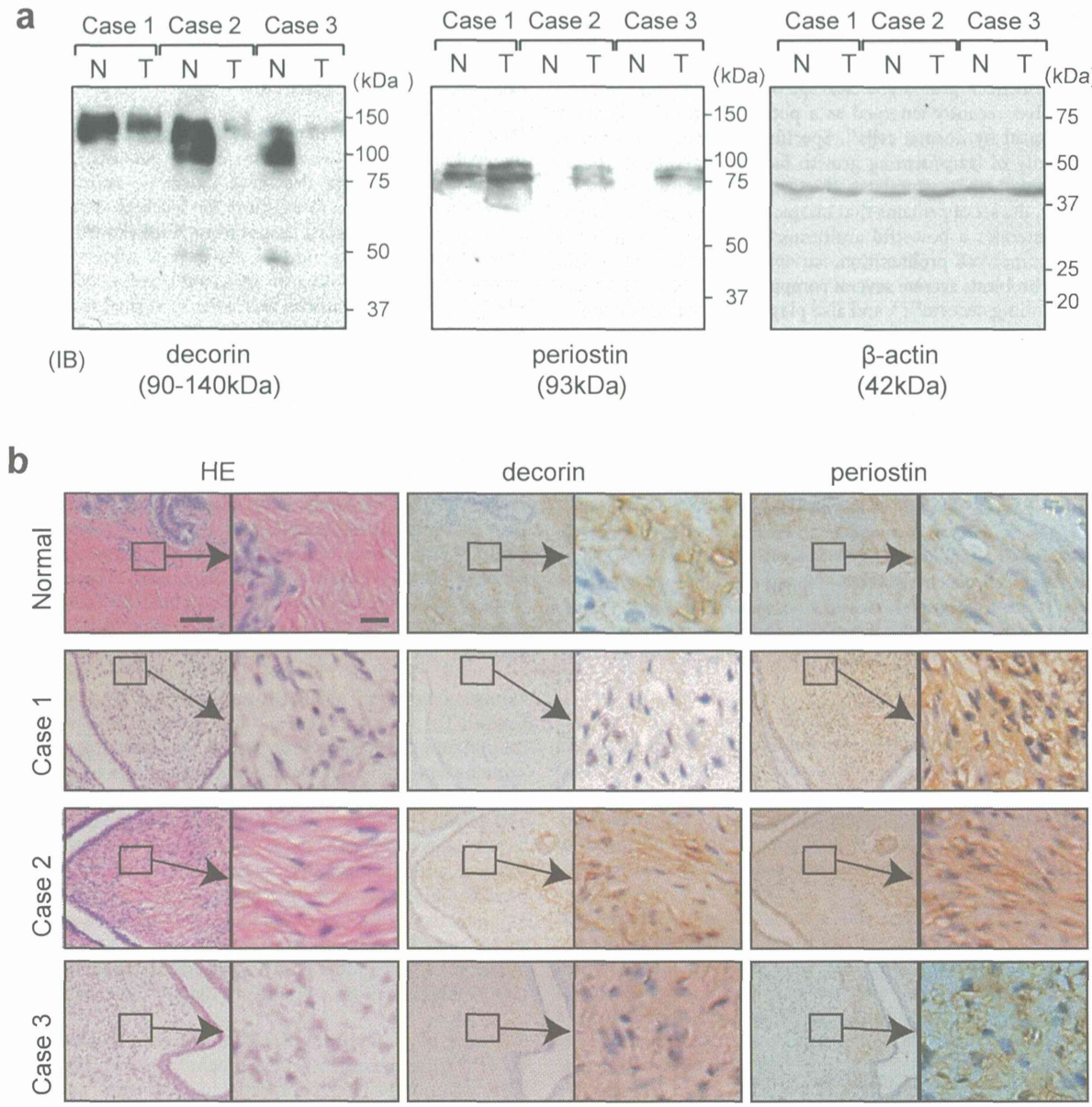

Figure 1 | Decorin and periostin expression levels in normal and tumor tissues. (a) Tissue lysates were immunoblotted with anti-decorin and anti-periostin antibodies. N, normal tissue; T, tumor tissue. (b) Tumor and normal tissues were fixed with formalin. Serial sections were visualized by hematoxylin and eosin staining (HE) and immunohistochemical staining with anti-decorin and anti-periostin antibodies. Bar = 100 μm. Insets indicate magnified views in right panel. Bar = 20 μm.

and Supplementary Figure S4 show an MRM transition for the co-eluting standard and endogenous peptides (VSPGAFTPLVK and DLPPDTTLLDLQNNK from decorin). In medium in which siRNA-periostin–treated cells were cultured, the spectrum peak corresponding to endogenous peptides overlapped with that of the standard peptide. However, in medium from siRNA-control–treated cells, there was no spectrum peak corresponding to endogenous peptides. On the other hand, periostin was detected by immunoblot analysis with anti-periostin antibody in medium from cells treated with siRNA-decorin cells, but not detected in medium from cells treated with siRNA-control or in non-transfected cells (Figure 3e). Next, we investigated whether MDA-MB-231 cells secrete decorin following decorin transfection, because these cells do not normally express decorin (Figure 3a). Figure 4b and Supplementary Figure S5 show two MRM transitions for the co-eluting standard and endogenous peptide (VSPGAFTPLVK from decorin). The decorin peptide sequence VSPGAFTPLVK was detected using nano-LC-MS/MS, and was determined at a 95% confidence level. We confirmed that the MS/MS spectrum of the peptide derived from secreted decorin was consistent with the decorin spectrum determined in normal tissue. This MRM-based assay demonstrated the high accuracy of target detection by MS/MS analysis (Figure 4c). The absolute quantitations are shown in Figure 4d. We calculated the concentration of decorin in cell-culture medium of siRNA-periostin–treated T47D cells and decorin-overexpressing MDA-MB-231 cells (n = 3). The levels of decorin in medium from siRNA-periostin–treated T47D cells and decorin-overexpressing MDA-MB-231 cells were 0.026 ± 0.007 nM and 0.699 ± 0.143 nM, respectively. The peaks of the endogenous peptide in each control were weak and non-detectable (ND).

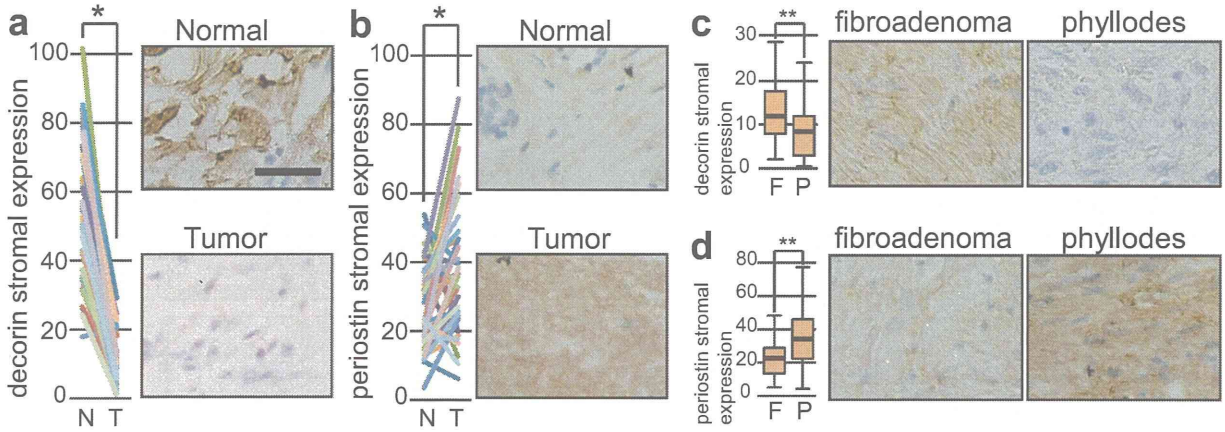

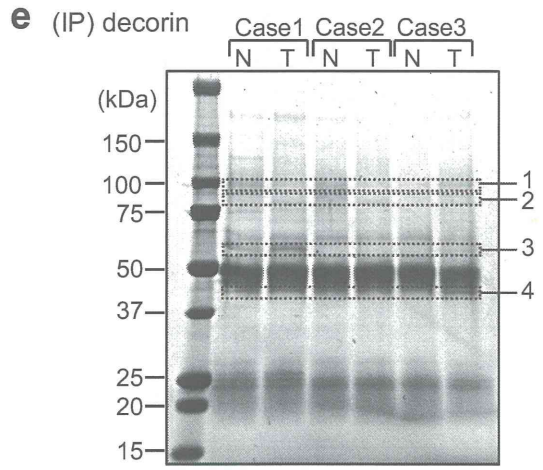

			Name	Unused	% Cov	Peptides (>95%)
1	Case1	Normal	Decorin	9.67	48.5	4
		Tumor	Decorin	4.06	48.2	1
	Case2	Normal	Decorin	14.06	53.8	7
		Tumor	Decorin	4.42	59.3	2
	Case3	Normal	Decorin	18.61	61.0	10
		Tumor	Decorin	14.1	50.1	7
2	Case1	Normal	Periostin	3.65	28.6	1
			Decorin	2.55	53.2	1
		Tumor	Periostin	11.45	43.4	5
			Decorin	7.19	28.1	3
	Case2	Normal	Decorin	20.75	46.5	13
		Tumor	Decorin	4.06	32.0	2
	Case3	Normal	Decorin	11.74	56.8	5
			Dermcidin	2.06	39.1	1
		Tumor	Hornerin	1.7	13.6	1

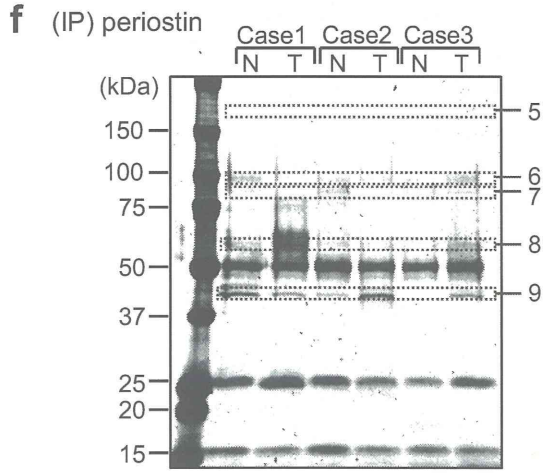

			Name	Unused	% Cov	Peptides (>95%)
6	Case1	Tumor	Decorin	4.26	31.8	2
	Case2	Normal	Decorin	28.51	73.8	16
		Tumor	Decorin	3.54	35.4	2
	Case3	Normal	Decorin	2.42	27.6	1
		Tumor	Decorin	13.7	39.6	5
7	Case1	Normal	Decorin	17.74	46.2	8
			Periostin	14.54	42.1	4
		Tumor	Periostin	25.97	55.1	10
			Decorin	4.15	34.3	2
	Case2	Normal	Decorin	41.92	53.2	23
			Periostin	3.55	22.4	1
		Tumor	Periostin	14.93	37.3	8
			Decorin	3.79	36.2	2
			Dermcidin	2.38	43.6	1
	Case3	Normal	Decorin	3.56	33.7	1
		Tumor	Decorin	7.84	37.9	3
			Periostin	5.42	33.1	2

Figure 2 | Comparison of stromal decorin and periostin expression levels and complex formation of both proteins in phyllodes tissues. (a, b) Normal tissues (N) and tumor tissues (T) from 35 phyllodes tumor patients were analyzed by immunohistochemical staining. Each colored line connects data points derived from one patient. (c, d) Stromal decorin and periostin expression levels in phyllodes tumors (P) (n = 35) were compared with those in fibroadenomas (F) (n = 37). The intensities of stromal decorin (a, c) and stromal periostin (b, d) expression were quantitated using the ImageJ software. (a)–(d) Figures alongside the graphs show representative samples from each group. Bar = 100 μm. (a, b) P values were determined using the Wilcoxon signed-rank test; $P < 0.05$ was considered to represent a statistically significant difference (*). (c, d) P values were determined using the Mann-Whitney U test; $P < 0.05$ was considered to represent a statistically significant difference (**).(e) Complex between periostin and decorin in normal and tumor tissues from phyllodes tumor patients. Anti-decorin immunoprecipitate in normal tissue (N) or tumor tissue (T) lysate from phyllodes tumor patients was subjected to SDS-PAGE, followed by silver staining. Gel bands representing differences between normal tissue and phyllodes tumor were cut out and subjected to in-gel trypsin digestion and mass spectrometry. Proteins identified from gel bands 1 and 2 are shown to the right of the SDS-PAGE image. Proteins identified from other bands are shown in Supplementary Table S2. (f) Anti-periostin immunoprecipitates in normal tissue (N) or tumor tissue (T) lysate from phyllodes tumor patients were subjected to SDS-PAGE, followed by silver staining. Proteins identified from gel bands 6 and 7 are shown to the right of the SDS-PAGE image. Proteins identified from other bands are shown in Supplementary Table S2.

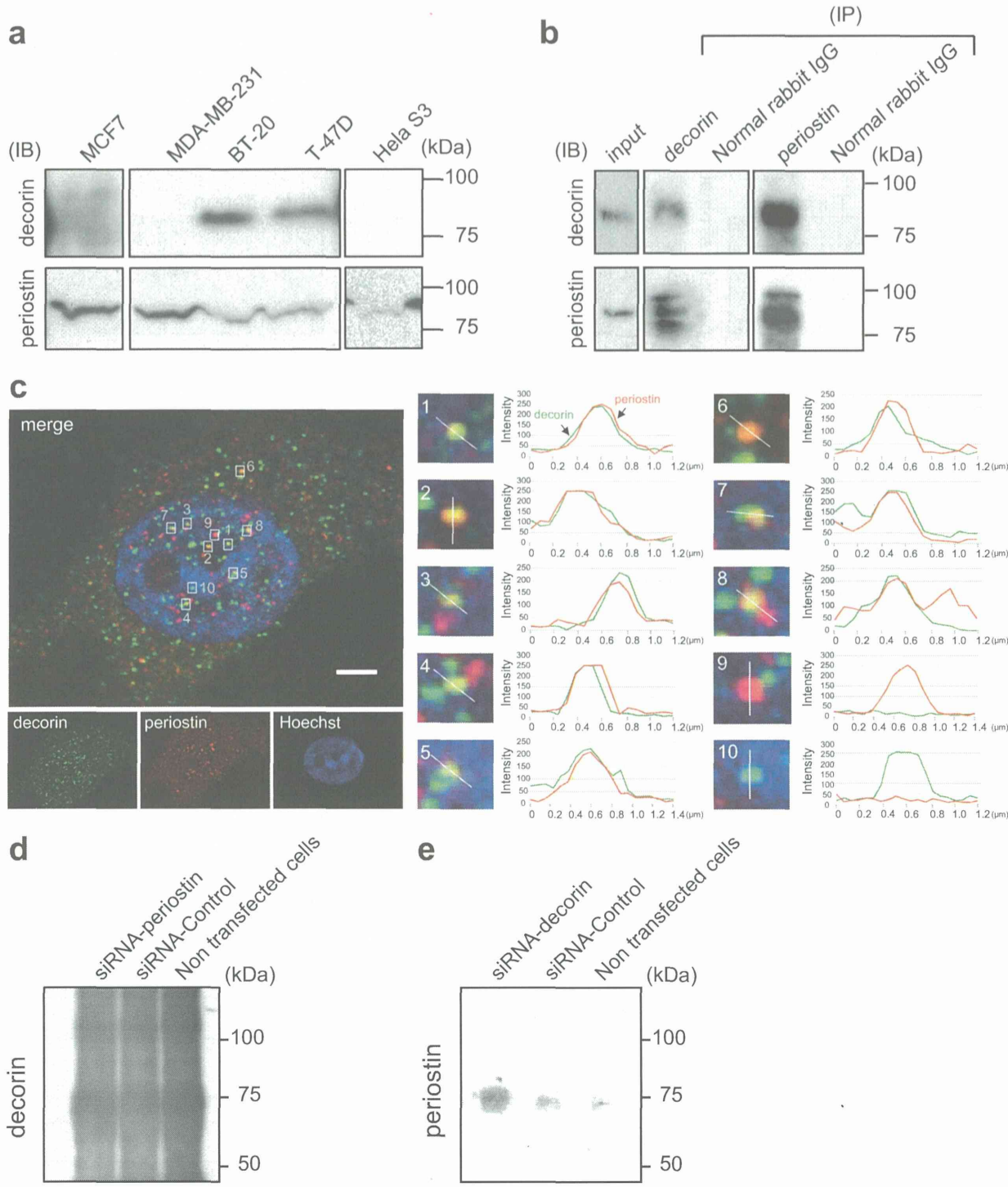

Figure 3 | Complex formation between decorin and periostin in BT-20 and T-47D cells. (a) The levels of expression of decorin and periostin in the breast cancer cell lines. Cell lysates from cancer cell lines MCF7, MDA-MB-231, BT-20, T-47D, and HeLa S3 were immunoblotted using anti-decorin and anti-periostin antibodies. Cropped blots are used in the main figures, and full-length blots are included in the supplementary information (Supplementary Figure S2) (b) Anti-periostin or anti-decorin immunoprecipitates from BT-20 cell lysates were subjected to SDS-PAGE, followed by immunoblot analysis with anti-decorin or anti-periostin, respectively. Input lysate was used as a positive control, and normal rabbit IgG was used as a negative control. Cropped blots are used in the main figures, and full-length blots are included in the supplementary information (Supplementary Figure S3) (c) BT-20 cells were fixed, permeabilized, and immunostained with anti-decorin (green) and anti-periostin (red). The cells were observed by high-resolution confocal microscopy on Leica TCS SP8 (left panel). Yellow shows the co-localization of decorin and periostin. Fluorescence intensity profiles along lines were drawn the staining patterns. Bar = 3 μm. Insets indicate magnified views in right panel. Decorin and periostin were closely merged. (d, e) We analyzed secreted decorin or periostin in culture medium of T-47D cells treated with siRNA-periostin (d) or siRNA-decorin (e) by immunoprecipitation, followed by immunoblotting using each antibody.